Energy Conversion and Management 263 (2022) 115655

Contents lists available at ScienceDirect

Energy Conversion and Management

journal homepage: www.elsevier.com/locate/enconman

High-performance triboelectric nanogenerator with synchronization mechanism by charge handling

Xin Yu [a,b], Jianwei Ge [a,b], Zhenjie Wang [a,b], Jianlong Wang [b], Da Zhao [b], Zhong Lin Wang [b,c,d,1], Tinghai Cheng [b,c,1,*]

[a] School of Electrical and Electronic Engineering, Changchun University of Technology, Changchun, Jilin 130012, China
[b] Beijing Institute of Nanoenergy and Nanosystems, Chinese Academy of Sciences, Beijing 101400, China
[c] CUSTech Institute of Technology, Wenzhou, Zhejiang 325024, China
[d] School of Materials Science and Engineering, Georgia Institute of Technology, Atlanta, GA 30332-0245, USA

ARTICLE INFO

Keywords:
Triboelectric nanogenerator
Synchronization mechanism
Flying capacitor
Energy harvesting
Charge handling

ABSTRACT

Triboelectric nanogenerator (TENG), as an effective environmental energy harvesting device, provides a promising method for powering electronic devices with low power consumption. However, the low surface charge density of the triboelectric layer limits its practical application. In this paper, a charge handling triboelectric nanogenerator (CH-TENG) with synchronous mechanism is proposed to effectively improve the output performance. It consists of the pump-TENG, the main-TENG, and charge handling circuit. Through the cooperation of the pump-TENG and charge handling module, the extra charges are injected into the main-TENG, rapid charge accumulation is achieved. The experimental results depict that CH-TENG obtains open-circuit voltage 1200 V, short-circuit current 75 μA, instantaneous output power 27 mW, and the transferred charge reaches 0.8 μC at a frequency of 1.5 Hz. Under the wind speed of 6 m/s, CH-TENG spent 39 s to charge the 220 μF capacitor to 3.0 V, and finally stabilized at 1.26 V to keep the hygrothermograph working stably. The CH-TENG provides a significant reference for improving the high-performance output harvest wind energy in the environment.

1. Introduction

With the booming development of sensor network, the portable electronic devices and distributed sensors have been universal in our products and lives [1–3]. The energy used to drive these devices will also rapidly increase [4,5]. The battery as a power source not only has a limited lifespan but also needs to face the environmental pollution problem caused by the difficulty of effective recycling. In order to reduce environmental pollution, rational development and utilization of energy, the development of clean and renewable energy and more efficient harvest is particularly important [6,7]. And how to effectively harvest energy in the environment and has attracted the attention of the majority of scientific researchers.

Triboelectric nanogenerator (TENG) was first invented by Wang's group in 2012 [8–12], it is based on the coupling effects of electrostatic induction and triboelectrification [13,14]. It has the characteristics of high conversion efficiency, a wide range of material selection, a simple production process, and low cost. It can effectively harvest the tiny energy in the environment and has attracted the attention of the majority of scientific researchers. At present, it has demonstrated great application development potential in four aspects of micro-nano energy, self-powered systems, blue-ocean energy, and high voltage applications [15,16]. But the surface charge density of TENG is still low triboelectric charging, which seriously affects the power output of the TENG [17–19]. In addition, the induced charge is limited to the surface of the dielectric layer, which is far from reaching its maximum charge output capacity [20–26]. Previous research aims to break through the limit of charge density, which is mainly focused on materials selection, structure optimization, surface modification, and environmental control of the TENG [27–32]. The above methods can maintain a high output performance [33–41]. However, the high-performance output is still difficult to achieve, due to the strictly environmental parameter control or the complex circuit parameters. For this reason, it is particularly important to design a high-performance output device with simple circuit parameters under normal circumstances.

In this work, a charge handling triboelectric nanogenerator (CH-

* Corresponding author at: Beijing Institute of Nanoenergy and Nanosystems, Chinese Academy of Sciences, Beijing 101400, China.
E-mail addresses: zhong.wang@mse.gatech.edu (Z.L. Wang), chengtinghai@binn.cas.cn (T. Cheng).
[1] The two authors have the same contribution to this study.

https://doi.org/10.1016/j.enconman.2022.115655
Received 11 January 2022; Received in revised form 17 March 2022; Accepted 17 April 2022

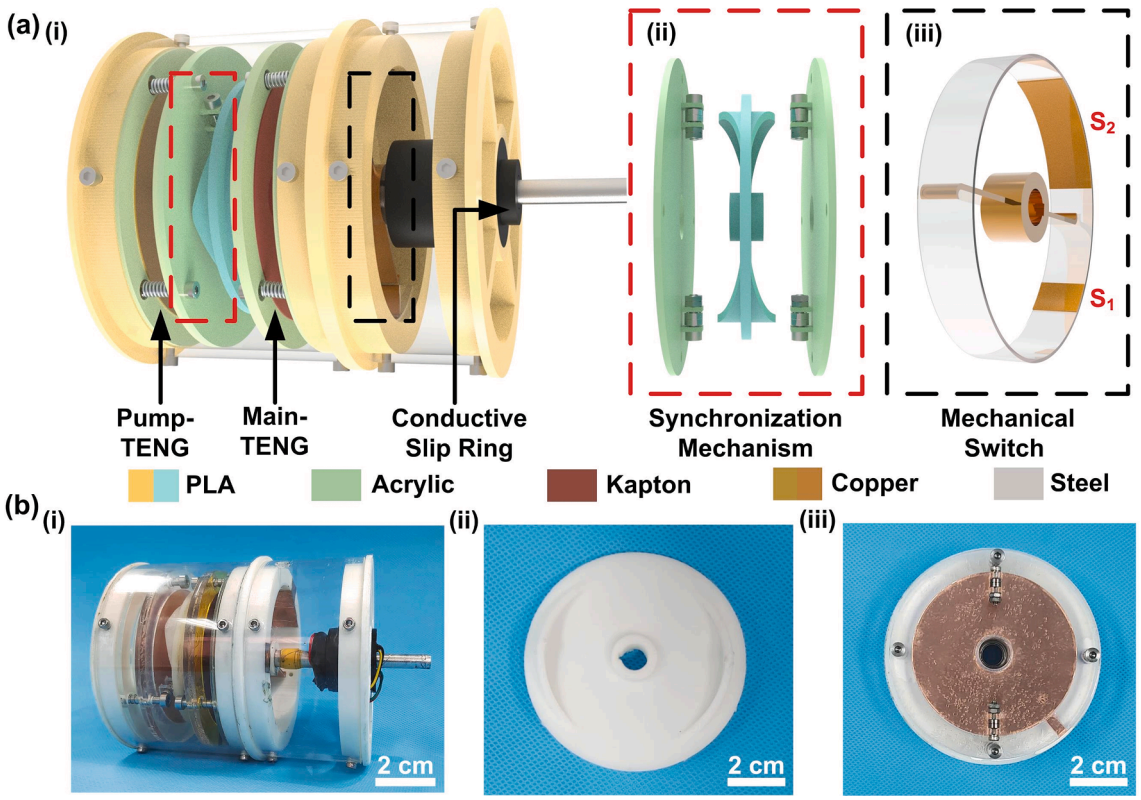

Fig. 1. (a) Overall rendering and main structure rendering of the CH-TENG. (i) Illustration of the overall structure; (ii) illustration of the synchronization mechanism; (iii) illustration of the contact switch. (b) Photographs of (i) the CH-TEHG; (ii) the cam in synchronization mechanism; (iii) the pump-TENG.

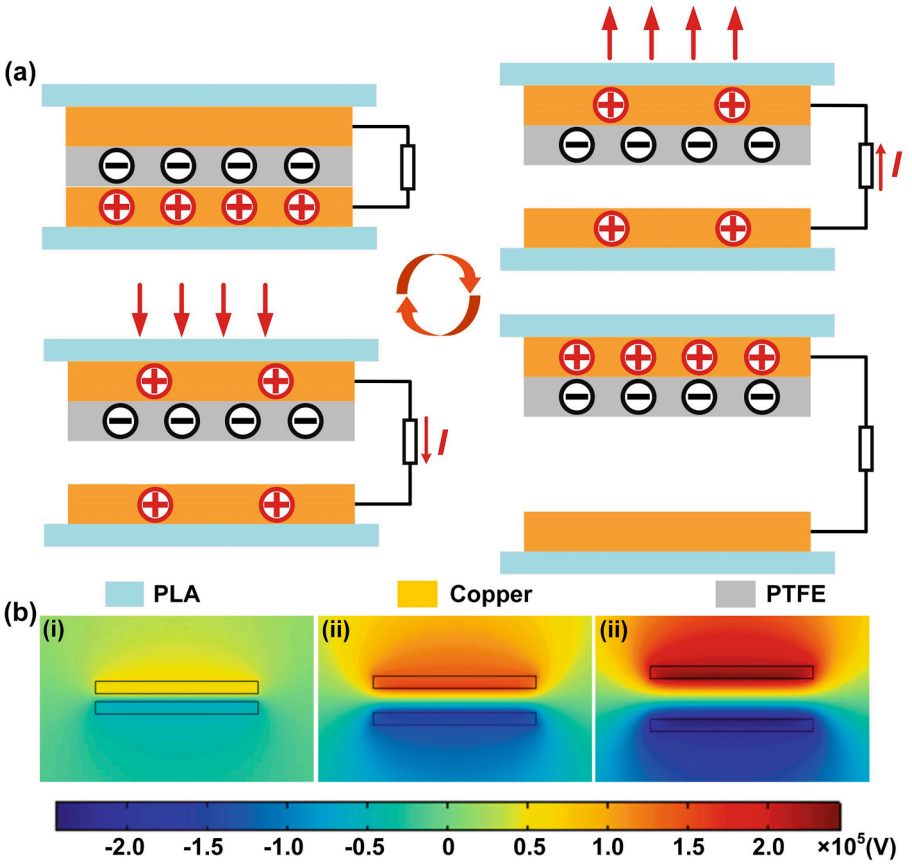

Fig. 2. Working principle of hardware equipment: (a) The working principle of contact separation TENG. (b) (i)-(iii) COMSOL potential simulation in three states.

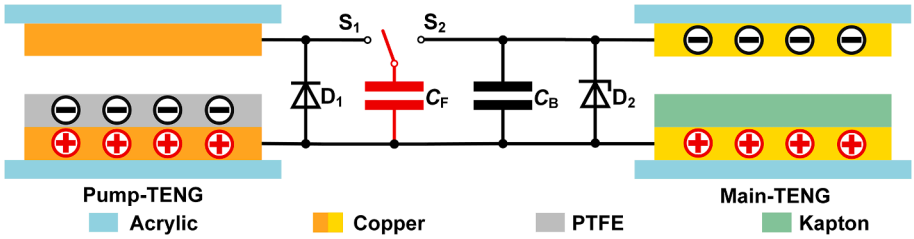

Fig. 3. The diagram of circuit working principle.

TENG) with synchronization mechanism is proposed. It consists of the pump-TENG, the main-TENG, and charge handling circuit, which includes a flying capacitor and mechanical switch. The pump provides charge and transfers it through the flying capacitor and mechanical switch in the charge handling module. The on–off of the switch matches the contact-separation movement of the TENG because of the mechanical switch. Therefore, the charge is injected from pump-TENG into the capacitor and main-TENG, and the multiple circulating charges reach maximum value. Meanwhile, the mechanical switch prevents charge backflow. The double capacitor value matches the TENG equivalent variable capacitor model of the contact-separation mode, which ensures to output the maximum charge of the main-TENG. The flying capacitor, buffer capacitance, and the number of regulated diodes is studied systematically impact on output performance. The CH-TENG prototype is driven at a frequency of 1.5 Hz, with an output open-circuit voltage of 1200 V, a short-circuit current of 75 μA, a charge transfer of 0.8 μC, and a power of 27 mW. Furthermore, it can stably actuate the temperature and humidity sensor in a simulated wind environment. In short, this work is about harvesting environmental energy, provides a new approach.

2. Structure design and operating principle

The assembly drawing of CH-TENG overall structure in Fig. 1a. The CH-TENG consists of the pump-TENG and the main-TENG in contact-separation mode, synchronization mechanism, a mechanical switch, and a conductive slip ring. Fig. 1a(i) depicts the complete schematic diagram of the prototype structure. Fig. 1a(ii) indicates the enlarged rendergraph of the synchronization mechanism. The synchronization mechanism is composed of four cams and two movers. The pump-TENG and the main-TENG are distributed on both sides of the synchronization mechanism. Also, the two movers of the synchronization mechanism are respectively pasted with Kapton film and PTFE film on the copper electrode. The module shaft rotates under excitation and drives the turntable in the synchronization mechanism to rotate. Then drives two separate TENG at the meantime under the action of the synchronization mechanism. And spring-driven TENG realizes contact separation movement at twice the external drive frequency. Fig. 1a(iii) shows the schematic diagram of the mechanical switch, and the mechanical switch consists of a rotor and a stator. The rotor is PLA, and its surface is covered with copper. When the rotor and the lower end of the stator copper foil contact, switch S_1 is turned on, and when the rotor and the upper end of the stator copper foil contact, switch S_2 is turned on. Fig. 1b(i) is the photograph of the CH-TEHG. Fig. 1b(ii)-(iii) respectively shows the cam in synchronization mechanism, and pump-TENG physical photo. Fig. S1(a)-(b) indicates the photo of Kapton and PTFE on the electrodes of two separate TENG.

As shown in Fig. 2(a), it shows the four states between the plates. The

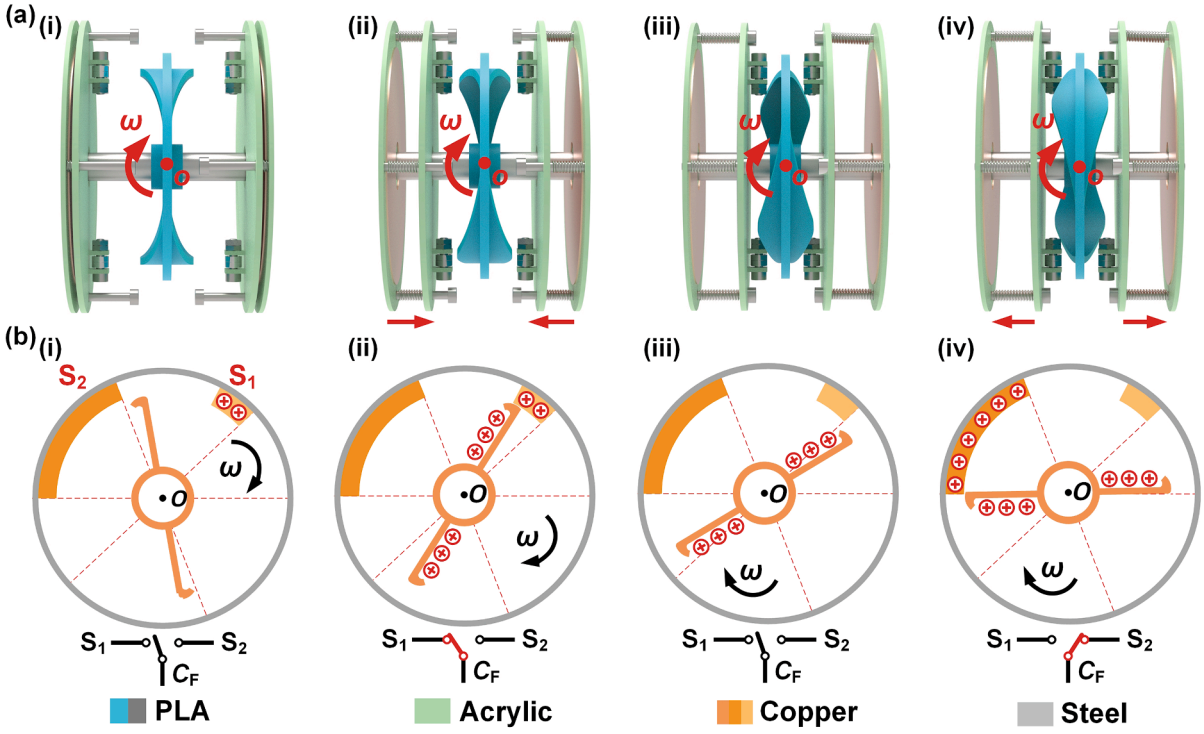

Fig. 4. (a) (i)-(iv) Four working process diagrams of the prototype. (b) (i)-(iv) Flow chart of turning on and off of mechanical switches S_1 and S_2.

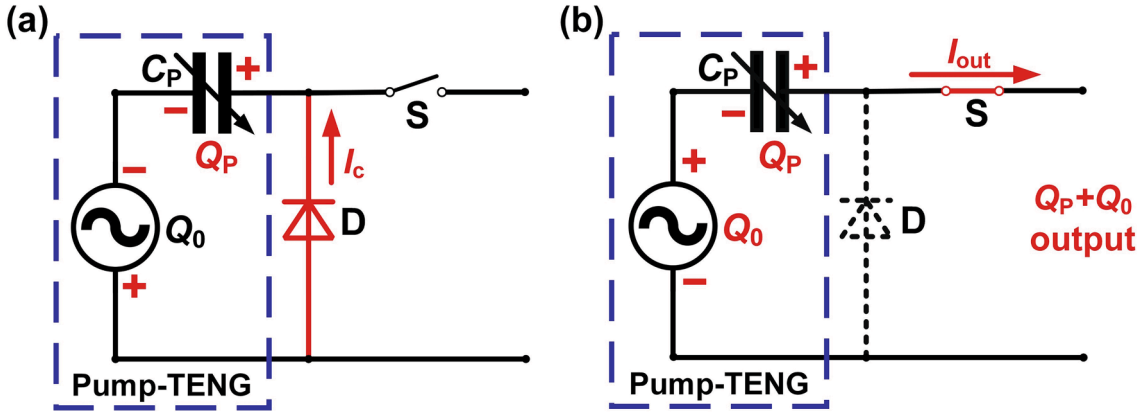

Fig. 5. Pump-TENG equivalent internal circuit working diagram: (a) charging process of an internal capacitor by the pump-TENG internal voltage source. (b) the pump-TENG internal voltage source and internal capacitor discharge process together.

charge does not transfer when in contact, and the electrons are transferred from the upper plate to the lower plate during separation. When the separation reaches the maximum value, the charges are balanced again, and the charges are not transferred. When approaching slowly, electrons are transferred from the lower board to the upper board. Fig. 2 (b) shows the change in the electric field intensity of the main-TENG plate during the contact separation process simulated by the COMSOL Multiphysics 5.5 software.

The equivalent circuit diagram of the CH-TENG is illustrated in Fig. 3. The circuit part in the middle contains a rectifier diode D_1, two capacitors (C_F and C_B) for charge transfer, and several Zener diodes D_2 for voltage stabilization.

As shown in Fig. 4, the working principle of the CH-TENG was demonstrated. Fig. 4a is the principle diagram of the four working states of the synchronization mechanism. During the rotation of the cam structure, two separate TENG realize the contact-separation movement synchronously. A cycle of synchronization mechanism work can be divided into four stages. As shown in Fig. 4a(i). It shows the first stage, at this time, the two plates of the TENG are in contact with each other. According to the parallel plate capacitance formula, the internal capacitance in main-TENG reaches the maximum value. In the second stage, as demonstrated in Fig. 4a(ii), the separation spacing between the two plates is about to reach the maximum at this time, and the pump-TENG voltage is about to reach the maximum. The third stage is depicted in Fig. 4a(iii), at this time, the separation spacing between the two plates reaches the maximum value, and the internal capacitance of the main-TENG is the smallest at present. The fourth stage is depicted in Fig. 4a(iv). The plate is just starting to close while the main-TENG capacitance gradually increases. When the cam structure rotates to drive the synchronization mechanism to contact and separate, the rotor of the mechanical switch also rotates at the same frequency. Fig. 4b contrasts the four changes of the mechanical switch. During this process, when the switch is disconnected from S_2, the plates are in contact, and they are about to separate to the maximum. Then the switch and S_1 are turned on. And at the moment of separation to the maximum distance, the switch is disconnected from S_1; when the two plates begin to close and meanwhile, the S_2 is on.

Based on the equivalent electrical characteristics of the TENG, it can be equivalent to a series connection of a voltage source and a variable capacitor [42–44]. For the contact-separation mode of TENG, the equivalent capacitance at complete contact and gradual separation is $C_{contact}$ and $C_{separate}$, which is shown in Eq. (1) and (2).

$$C_{contact} = \frac{\varepsilon_0 \varepsilon_r S}{d} \tag{1}$$

$$C_{separate} = \frac{\varepsilon_0 S}{\frac{d}{\varepsilon_r} + x} = \frac{\varepsilon_0 \varepsilon_r S}{d + \varepsilon_r x} \tag{2}$$

where d and ε_r are the thickness and relative dielectric constant of the dielectric material, S is the effective contact area of two plates, x is the distance between the layers of triboelectric, here x is restricted in the interval of [0, 8 mm], ε_0 is the vacuum dielectric constant.

For the pump-TENG, considering its equivalent circuit model, as shown in Fig. 5a, in the first stage, when the TENG comes into contact

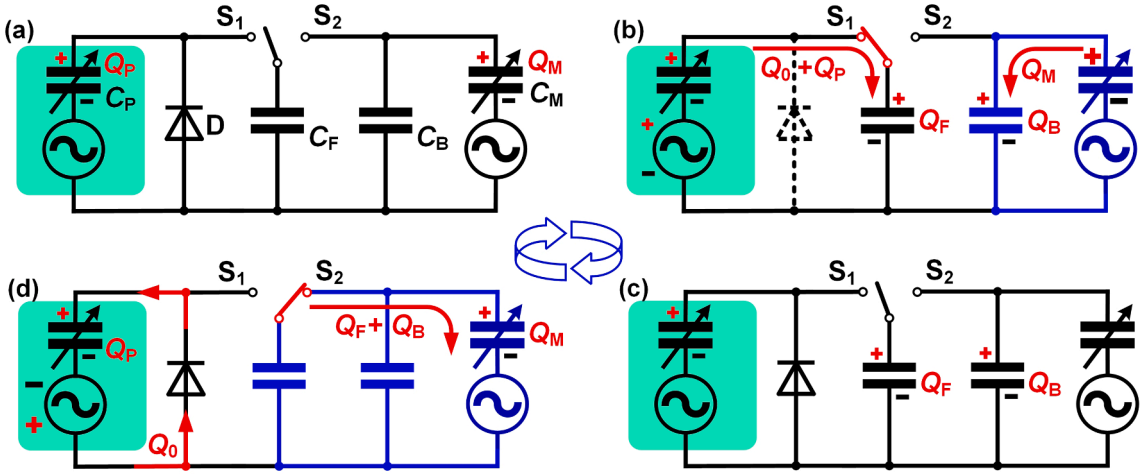

Fig. 6. (a)-(d) Equivalent circuit model and charge transfer process diagram.

gradually, because the potential of the lower plate of TENG is higher than that of the upper plate, the diode D is short-circuited, and the switch S is turned off, and the equivalent capacitance of the TENG reaches the maximum due to the reduction of the air gap, and the charge Q_0 is stored in C_P in the form of charge Q_P through the diode. As shown in Fig. 5b, in the second stage, When the TENG plate distance is about to separate to its maximum, the potential of the lower plate is now lower than that of the upper plate. At this time, the diode D is conductive, the switch is off, the capacitance of the main-TENG equivalent capacitor decreases due to the increase of air gap, and the charge Q_0 in the voltage source and the charge Q_P buffered in the capacitor C_P is simultaneously outputting to the circuit.

The equivalent charge transfer diagram of the CH-TENG is demonstrated in Fig. 6, which is consistent with the above-mentioned synchronization mechanism and switching process. It is divided into four working stages. Here, in order to briefly discuss the charge transfer situation, all charges are transferred by default all at once. In the first stage, when the two plates are in contact, the internal capacitance C_P in the pump-TENG is charged to Q_P by the internal voltage source of the pump-TENG through the rectifier diode. And the internal equivalent capacitance C_M of the main-TENG increases to the maximum, the stored charge in the main-TENG reaches the maximum value Q_M. At this point, C_M is in the second stage. At the moment when the distance between the two plates is going to reach the maximum value, switch S_1 is off. At this time, the voltage of the pump-TENG is about to reach the maximum value, and the generated charge Q_0 is released instantaneously after the accumulation of the charge Q_P of the internal capacitor and charges the flying capacitor C_F to the charge Q_F. At this time, the capacitance C_M of the main-TENG decreases sharply due to the separation of the plates, and the charge Q_M is transferred to the buffer capacitor C_B, which would be stored as a charge Q_B. In the third stage, When the separation distance between the two plates reaches the maximum, the switch S1 is turned off at the same time, with a stable charge and no-occurring transfer. The charges are all stored in the capacitors C_F and C_B, their charges are Q_F and Q_B respectively. In the fourth stage, the two plates begin to close, and the switch S_2 is off as well. At this time, the voltage source in the pump-TENG self-charges its internal capacitor C_P to charge Q_P via rectifying diodes. As the equivalent capacitance inside the main-TENG gradually increases, the charges Q_F and Q_B in the capacitors C_F and C_B are jointly transferred to C_M and stored in the charges Q_M. At this time, a cyclic pumping process is completed.

After charge excitation on the main-TENG, air breakdown occurs due to excessive the voltage V_{TENG} between the dielectric layer of the upper and lower electrodes. According to Paschen's Law, it is very important to calculate the maximum charge according to the main-TENG dielectric parameters. In the main-TENG separation process, $V_{TENG} = V_B$. Q is the total transferred charge, $Q(x)$ is the charge of the triboelectric layer at a separation distance of x. The charge of C_B is equal to $Q_B = Q\text{-}Q(x)$.

$$\frac{Q_{TENG}}{C_{TENG}} = \frac{Q_B}{C_B} \tag{3}$$

$$\frac{Q(x)}{\frac{\varepsilon_0\varepsilon_r S}{d+\varepsilon_r x}} = \frac{Q - Q(x)}{C_B} \tag{4}$$

$$Q(x) = \frac{Q\varepsilon_0\varepsilon_r S}{C_B(d+\varepsilon_r x) + \varepsilon_0\varepsilon_r S} \tag{5}$$

According to Paschen's Law, the relationship of the breakdown voltage and the gap distance is:

$$V_P = \frac{A(Px)}{\ln(Px) + B} \tag{6}$$

where P is the pressure of the gas, A and B are the constants determined by the composition and the pressure of the gas. In order to avoid air breakdown effect, $V_{TENG} < V_P$.

Table 1
Parameters of CH-TENG used in numerical analysis.

Name	Symbol	Numerical value
Constant	A	43.66
Constant	B	12.8
Atmospheric pressure	P	1.013×10^5 Pa
Effective contact area	S	4.77×10^{-3} m^2
Dielectric material thickness	d	5×10^{-5} m
Relative permittivity of dielectric materials	ε_r	3.4
Vacuum dielectric constant	ε_0	8.854×10^{-12}
Buffer capacitor	C_B	6.8×10^{-9} F

In order to avoid air breakdown, the governing equation of Q should be given. Combined with Eqs. (4)-(6), the governing equation of Q is established:

$$Q = \frac{A(Px)C_B}{\ln(Px) + B} + \frac{A(Px)\varepsilon_0\varepsilon_r S}{(\ln(Px) + B) \times (d + \varepsilon_r x)} \tag{7}$$

In order to illustrate the change rate of Q, the derivative of Q with respect to x is given:

$$\frac{dQ}{dx} = \left(\frac{AP}{\ln(Px) + B} - \frac{AP}{(\ln(Px) + B)^2}\right) \times \left(C_B + \frac{\varepsilon_0\varepsilon_r S}{d + \varepsilon_r x}\right) - \frac{APx}{\ln(Px) + B} \times \frac{\varepsilon_0\varepsilon_r^2 S}{(d + \varepsilon_r x)^2} \tag{8}$$

The numerical parameters in Eq. (7) and Eq. (8) are listed in Table 1. The numerical analysis process is provided in Supplementary Note 1 (Supporting Information), the numerical analysis results illustrate that when the distance x is reached at 8 mm, the amount of Q_{max} is 12.3 μC. Therefore, in order to effectively avoid air breakdown, in experiment, the transferred charge Q_{sc} should be less than 12.3 μC.

3. Experimental section

3.1. Fabrication of the CH-TENG

The CH-TENG is composed of an aluminum shaft, two barrels, bearings, springs, acrylic plate as electrode base, cam, a mechanical switch, conductive slip ring, copper electrode, flexible film, and base. Four pieces of acrylic plates with dimensions of 102 mm (outer diameter) × 15 mm (inner diameter) × 2.5 mm (height) are processed by laser cutting machine as bases. For two acrylic plates, they are pasted with the copper electrode with a sponge of a size of 80 mm (external diameter) × 18 mm (inner diameter) × 1.0 mm (height). The other two acrylic plates are pasted with copper electrodes and covered with 50 μm Kapton and 130 μm Poly tetra fluoroethylene (PTFE), respectively. The contact area between them and the copper electrode is 80 mm (external diameter) × 18 mm (inner diameter). The lengths of the two drums are 74 mm and 40 mm, respectively. Their specific size is 110 mm (external diameter) × 104 mm (inner diameter). The size of the spring that makes the two contact electrodes spring apart is 0.3 mm (wire diameter) × 5.0 mm (external diameter) × 15 mm (length). The cam, base, end caps, and mechanical switches on the mechanical structure are print through a 3D printer, the material is polylactic acid (PLA). A lathe processes the aluminum shaft. The circuit consists of 3 kV ceramic capacitor, buffer capacitors (CBB81), rectifier diodes (1N4007), and Zener diodes (3EZ400D5).

3.2. Electrical measurement

The rotary motor (J-5718HBS401, Longshun, China) is used to drive the CH-TENG as the input source, keeps the CH-TENG stable output. The transferred charges and the short-circuit current were measured by a programmable electrometer (6517B, Keithley, USA) and a data

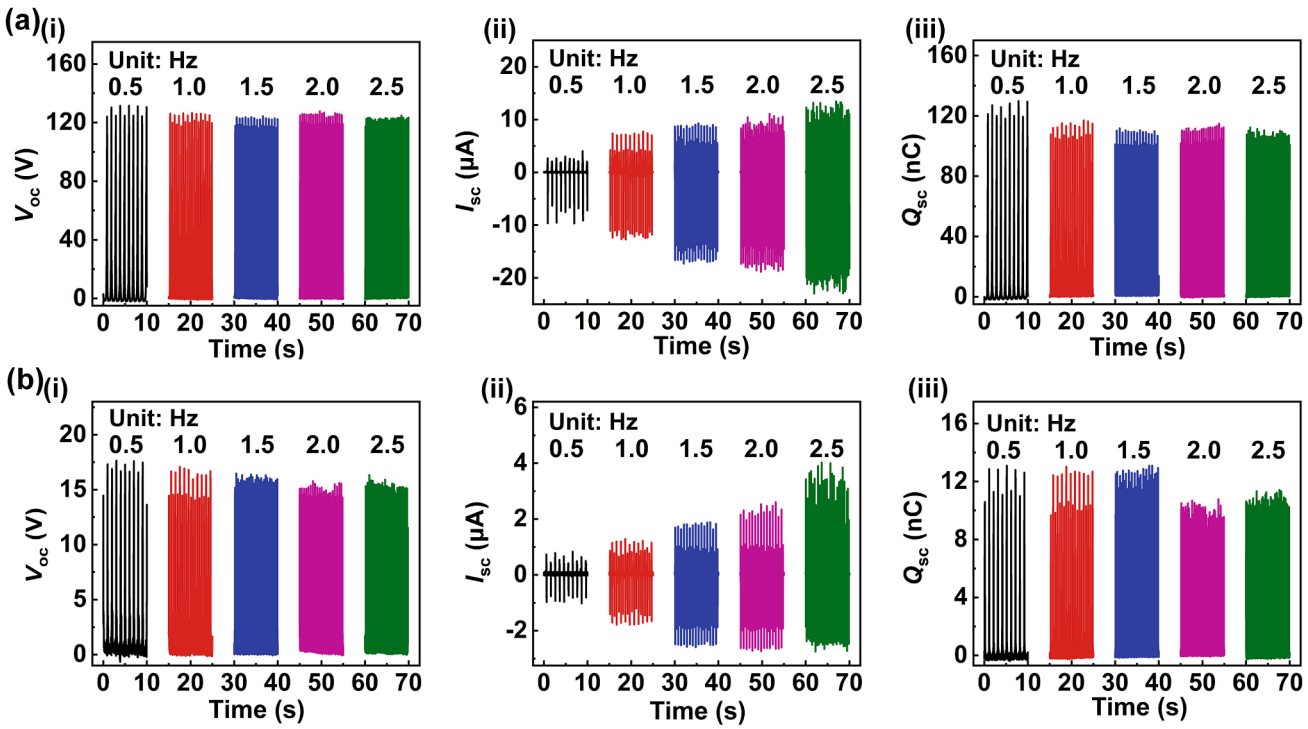

Fig. 7. Initial output performance: (a) (i)-(iii) Voltage, current, and charge of Pump-TENG at different frequencies. (b) (i)-(iii) Voltage, current, and charge of Main-TENG at different frequencies.

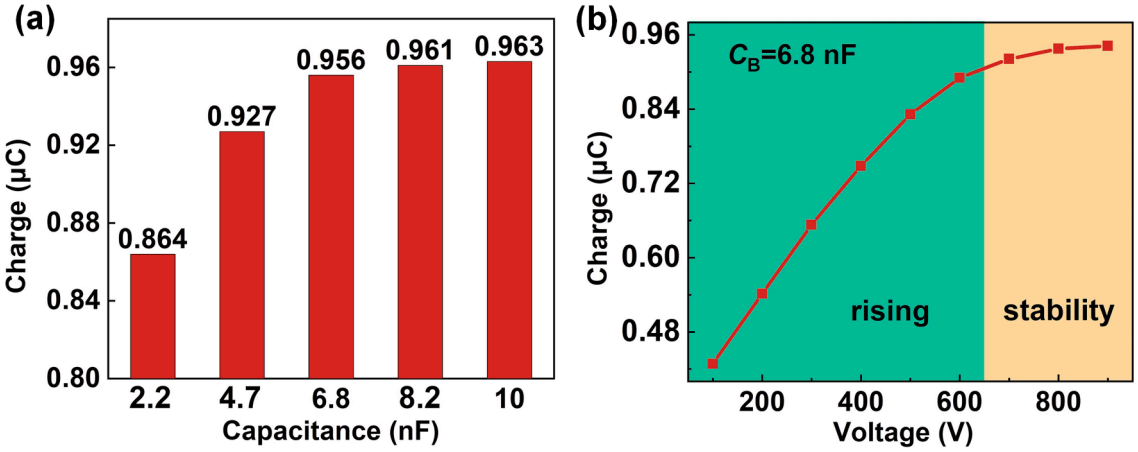

Fig. 8. (a) The CH-TENG maximum pumping amount of different buffer capacitors with voltage source. (b) Pump charge of 6.8 nF buffer capacitor at different voltages.

acquisition system (PCI-6259, National Instruments, USA) test. And a source meter (6517B, Keithley, USA) was adopted as the voltage source for providing excitation voltage. A super phosphor oscilloscope (SDS2204X, Siglent, China) is used to measure the open-circuit voltage.

4. Results and discussion

In the overall prototype test, to better understand the effect of two separate TENG performance on the output performance of CH-TENG, as well as the best frequency relationship of double TENGs. As shown in Fig. 7, measured the initial performance output of two separate TENG systematically. Eliminating the influence of excessively high frequency on the stability of the synchronization mechanism, the initial performance output of two separate TENG have the same trend. In order to ensure the stability of the experiment, the frequency of 1.5 Hz is adopted for the subsequent experiment. In the subsequent experiments, under the influence of the static charge on the surface of the main-TENG, the initial voltage output of the main-TENG at 1.5 Hz is 16 V, the current output is 2.5 μA, and the charge output is 13 nC.

In order to systematically discuss the influence of the specific parameters of each device in the circuit on the output of CH-TENG. A high voltage source is adopted instead of pump-TENG and flying capacitor to provide input voltage, the charge is injected into the main-TENG and buffer capacitor shows in Fig. 8. The transferred charge of the main-TENG reached the steady-state value in an instant using a high voltage source. Theoretically. As the buffer capacitor size increases, the amount of charge transferred between the main-TENG and the buffer capacitor increases gradually in each cycle. As shown in Fig. 8a, this article tested different buffer capacitors undermatching. Maximum buffer charge under excitation of different voltage sources. But when the pump-TENG

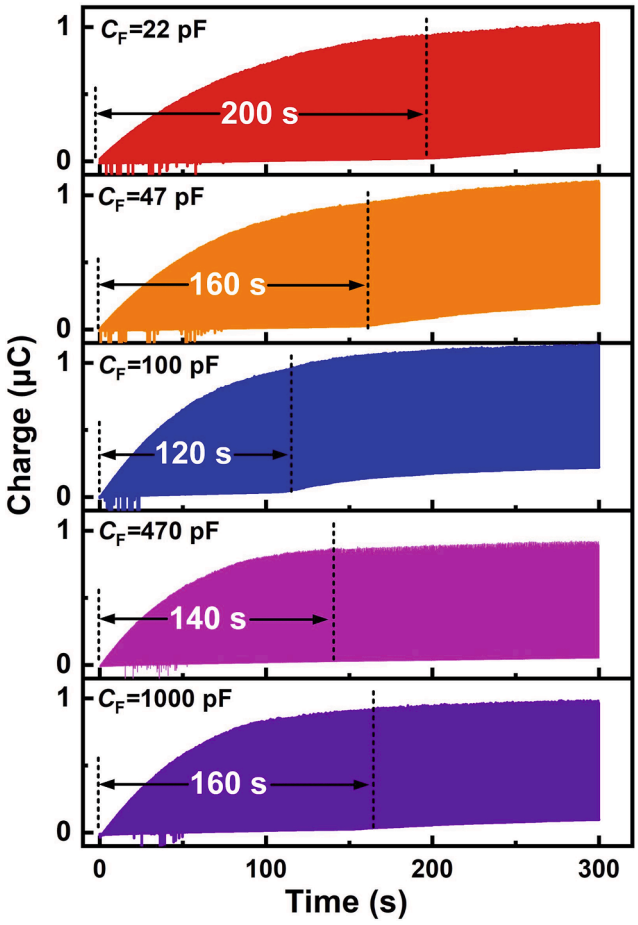

Fig. 9. The time for CH-TENG to transferred charge to saturation under different flying capacitances.

input excitation value is constant, the larger the buffer capacitance value is, the longer the charging time will be, but the final charge transferred by the main-TENG will not change significantly. Finally, a 6.8 nF buffer capacitor is used for subsequent performance measurement experiments to achieve the fastest charging time. Fig. 8b illustrates that the buffer the graph of the buffer charge with the voltage of the voltage source when a 6.8 nF buffer capacitor is used. The buffer charge at the beginning rises linearly with the increase of the voltage and then tends to be saturated.

After determining the maximum transferred charge and buffer capacitance were determined in the above experiments. When the pump-TENG input is fixed, another key issue is the saturation time for main-TENG to reach its maximum output. The flight flying capacitor and buffer capacitor of the main-TENG determine the time at which the charge reaches saturation output. According to the capacitive reactance matching principle, when the flying capacitor is small enough relative to the main-TENG, there can be a greater proportion of the charge that can be pumped into the main-TENG by the flying capacitor. Still, if the capacitance is small enough, the amount of charge pumped each time will also decrease. As shown in Fig. 9, the time for charge to reach dynamic saturation under different flying capacitor was tested. As the value of flying capacitor increases, so does the amount of charge transferred in each cycle of the main-TENG, and the speed of charge transfer gradually increases. The transfer speed reaches the maximum when the flying capacitor is 100 pF, and it spends 120 s to reach the main-TENG charge. When the charge approaches saturation, the capacitance value of the flying capacitor continues to increase. Due to the capacitance matching, the charge transferred from the flying capacitor to the main-TENG gradually decreases, and most charge is stored in the flying capacitor. Therefore, as the capacitance continues to increase, the speed of charge transfer gradually decreases.

In the above experiments, the values of buffer capacitance and flying capacitor in the circuit are determined by testing the maximum pumping charge and the shortest pumping time. However, The saturated charge output will continue to drift upward due to air breakdown, as shown in Fig. 10a. Fig. 10b depicts the initial and final charge accumulation process. In order to avoid the effects of air breakdown, the voltage at both ends of the main-TENG is stabilized at a certain value. It connects Several Zener diodes are connected in parallel at both ends, the influence of the number of Zener diodes on the output charge is also explored, as shown in Fig. 10c, with increasing the number of Zener diodes, the amount of transferred dynamic charge first increases and then decreases. The reason is that as the number of Zener diodes increases, the stabilized voltage gradually increases. However, due to the large loss of the Zener diodes used, when there are more than three Zener diodes, not only there is no voltage stabilizing effect, but the amount of charge transferred will also be reduced due to loss. Finally, determined to choose three Zener diodes to keep the voltage stable and the output charge reaches a maximum value, shown in Fig. 11. And the output charge under one and two Zener diode shown in Fig. S2(a)-(b). Fig. 11a depicts the amount of charge is transferred by three Zener diodes, which gradually keep stable after reaching the maximum value. Fig. 11b depicts the charge amplification output at the beginning and ending with the use of three Zener diodes.

5. Demonstration

After determining the circuit parameters, Fig. 12 illustrates the voltage and current output at 1.5 Hz and a zoomed-in end view. The output current is 75 μA and the output voltage is about 1200 V. As voltage does not change with frequency, but frequency affects the output

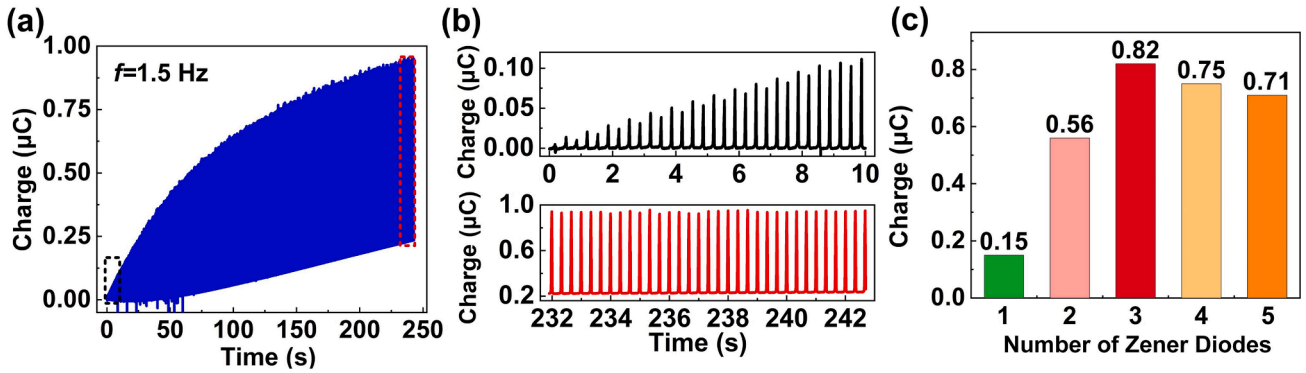

Fig. 10. (a) The dynamic charge output of CH-TENG in the absence of zener diodes. (b) Enlarged view of charge accumulation curves, initial values (up), and saturation values (down). (c) Influence of a different number of Zener diodes on pumped charge.

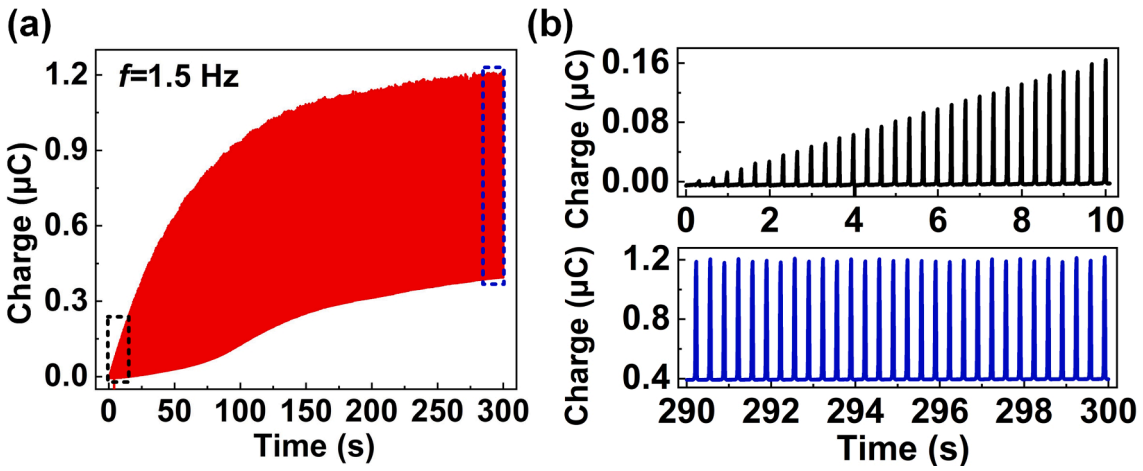

Fig. 11. (a) The dynamic charge output of CH-TENG is in the case of zener diode. (b) Enlarged view of charge accumulation curves, initial values (up), and saturation values (down).

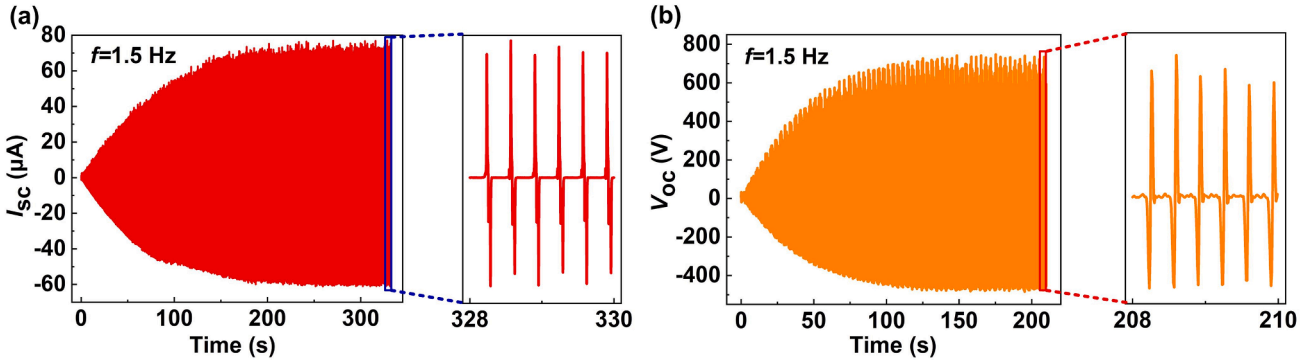

Fig. 12. (a) The CH-TENG output current. (b) The CH-TENG output voltage.

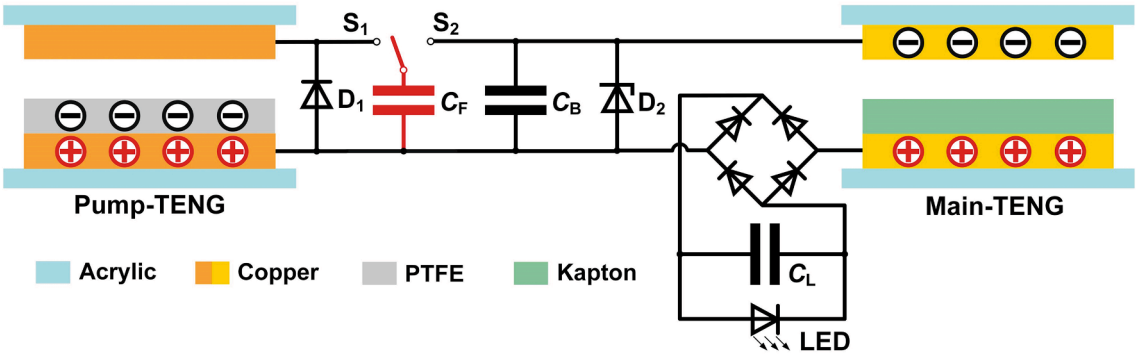

Fig. 13. Integrated equivalent circuit diagram for powering electronic equipment.

current. The changes of current at 0.5, 1.0, 2.0 and 2.5 Hz are shown in Fig. S3.

Besides, since CH-TENG produces an output of alternating current (AC), the output is converted to direct current through a full-bridge rectifier circuit and power the load device, as shown in Fig. 13. In addition, the peak power output of the CH-TENG operating at different load resistances at 1.5 Hz is also measured. When choosing a matching resistor of 10 MΩ, the peak power reaches 27 mW, as shown in Fig. 14a. Fig. 14b presents the time-dependent changes of capacitor voltage when CH-TENG charges different capacitors.

In addition, the CH-TENG lights up 320 LEDs, as shown in Fig. 15a (i)-(ii) and Supporting Video 1. Moreover, the commercial performance of CH-TENG is demonstrated in Fig. 15b(i). The commercial hygrothermograph can be powered normally in the simulated wind speed of 6 m/s wind environment. The specific working process is demonstrated in Supporting Video 2. Fig. 15b(ii) illustrates the voltage change process of the capacitor supplying power to the sensor. The CH-TENG charges 220 μF external capacitor to 3.0 V, the voltage is stabilized at 1.26 V when power is supplied, and the hygrothermograph is continuously and stably powered.

6. Conclusions

In this work, a high-performance output of the CH-TENG is proposed,

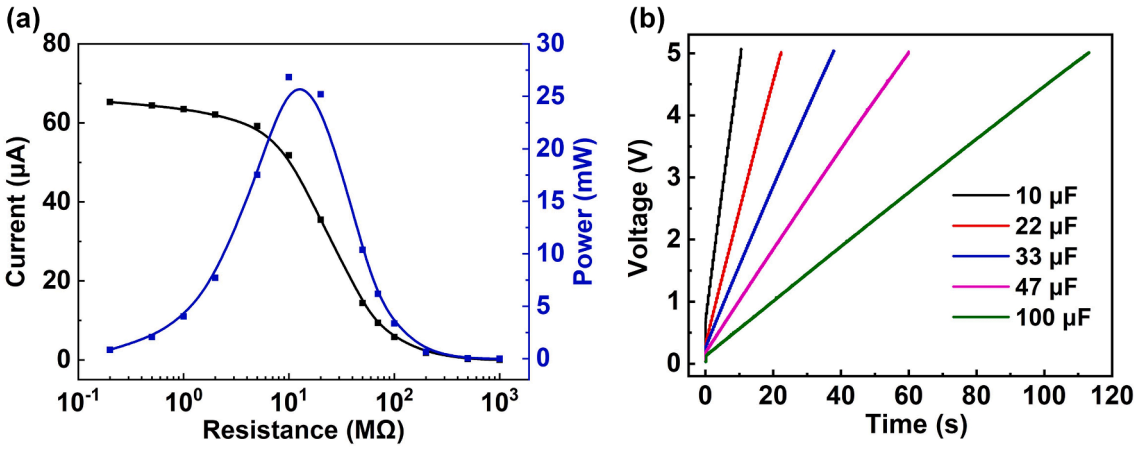

Fig. 14. (a) Output current and output power of the CH-TENG operating at different loads. (b) Charging curves for different external capacitors.

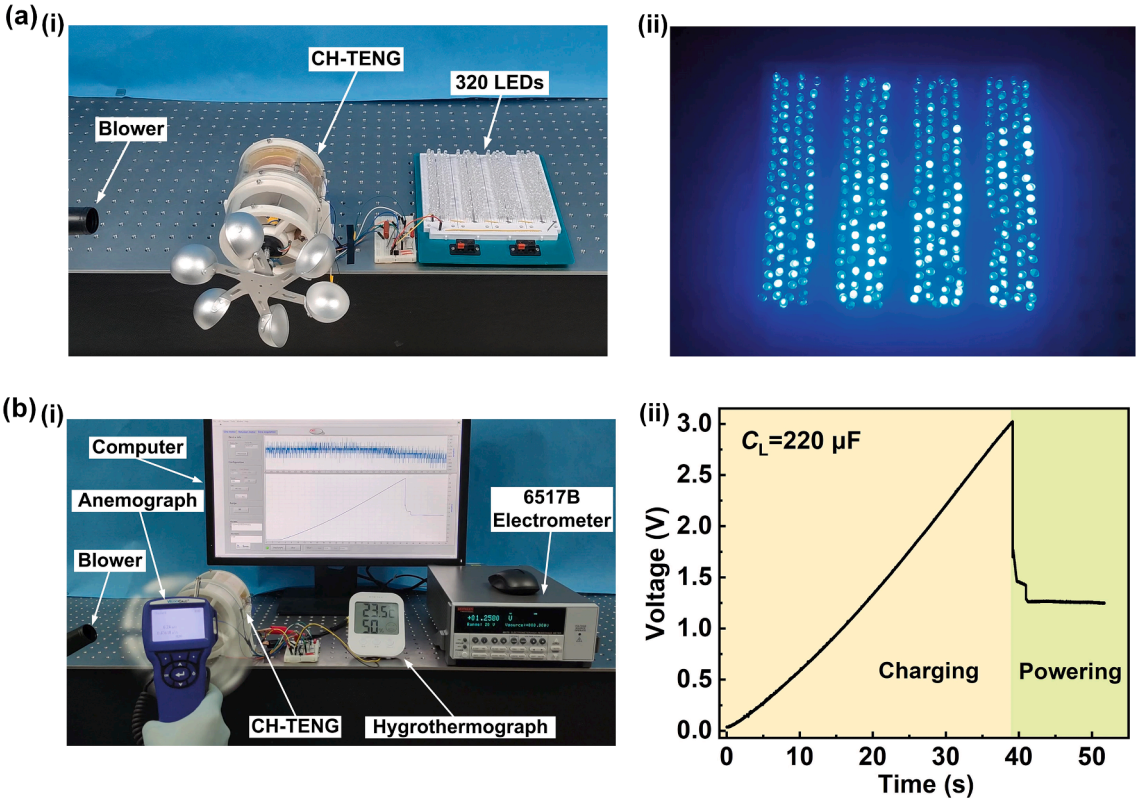

Fig. 15. (a) (i)-(ii) The CH-TENG lights up about 320 light-emitting diode (LED) lights in the wind environment. (b) (i) the CH-TENG lights up the hygrothermograph in the wind environment; (ii) voltage curve of load capacitor supplying power to the hygrothermograph.

for efficient harvesting of wind energy in conventional environments, which illustrates good application prospects. Transferring the charge through the charge handling module to achieve high-performance output. This method introduces two charge transfer mechanisms, one for the flying capacitor to pump the output charge of the pump-TENG, and the other is used for charge transfer between main-TENG discharge and buffer capacitance. The mechanical switch is matched with the TENG contact-separation movement, which solves the problems of rapid charge injection and prevention of charge backflow. By constructing the equivalent variable capacitance model of the TENG, it is matched with the flying capacitor and buffer capacitor. Finally, the CH-TENG can generate 1200 V, 75 μA, 0.8 μC, and 27 mW under the frequency of 1.5 Hz. And the hygrothermograph can be stably powered in the simulated wind environment. The CH-TENG adopts charge processing circuit to deal with accumulated charge, which significantly improves the output performance of TENG in wind environment.

CRediT authorship contribution statement

Xin Yu: Conceptualization, Investigation, Writing – original draft. **Jianwei Ge:** Investigation, Writing – original draft. **Zhenjie Wang:** Investigation, Validation. **Jianlong Wang:** Investigation. **Da Zhao:** Investigation. **Zhong Lin Wang:** Conceptualization, Resources, Writing – review & editing, Supervision. **Tinghai Cheng:** Conceptualization, Resources, Writing – review & editing, Supervision.

Declaration of Competing Interest

The authors declare that they have no known competing financial interests or personal relationships that could have appeared to influence the work reported in this paper.

Acknowledgments

The authors are grateful for Scientific Research Project of Education Department of Jilin Province (JJKH20210736KJ), the Science and Technology Innovation and Entrepreneurship Project for Overseas Scholars (2021-118-QD-1), and the Beijing Natural Science Foundation (No. 3222023).

Appendix A. Supplementary data

Supplementary data to this article can be found online at https://doi.org/10.1016/j.enconman.2022.115655.

References

[1] Chen J, Wang ZL. Reviving vibration energy harvesting and self-powered sensing by a triboelectric nanogenerator. Joule 2017;1:480–521. https://doi.org/10.1016/j.joule.2017.09.004.
[2] Wang ZL. Entropy theory of distributed energy for internet of things. Nano Energy 2019;58:669–72. https://doi.org/10.1016/j.nanoen.2019.02.012.
[3] Wang ZL. Triboelectric nanogenerator (TENG)—sparking an energy and sensor revolution. Adv Energy Mater 2020;10:2000137. https://doi.org/10.1002/aenm.202000137.
[4] Rahman M, Oni A, Gemechu E, Kumar A. Assessment of energy storage technologies: A review. Energy Convers Manag 2020;223:113295. https://doi.org/10.1016/j.enconman.2020.113295.
[5] Sánchez A, Zhang Qi, Martín M, Vega P. Towards a new renewable power system using energy storage: An economic and social analysis. Energy Convers Manag 2022;252:115056. https://doi.org/10.1016/j.enconman.2021.115056.
[6] Li Y, Wang S, Zhao Y, Yue L. Experimental study on the effect of core flow heat transfer enhancement on the performance of TEG. Energy Rep 2022;8:575–80. https://doi.org/10.1016/j.egyr.2021.11.218.
[7] Fatih S, Hakan F. Identification of pulsating flow effects with CNT nanoparticles on the performance enhancements of thermoelectric generator (TEG) module in renewable energy applications. Renew Energ 2020;162:1076–86. https://doi.org/10.1016/j.renene.2020.07.071.
[8] Wang ZL, Song J. Piezoelectric nanogenerators based on zinc oxide nanowire arrays. Science 2006;312:242–6. https://doi.org/10.1126/science.1124005.
[9] Fan F, Tian Z, Wang ZL. Flexible triboelectric generator. Nano Energy 2012;1:328–34. https://doi.org/10.1016/j.nanoen.2012.01.004.
[10] Zhang C, Tang W, Han C, Fan F, Wang ZL. Theoretical comparison, equivalent transformation, and conjunction operations of electromagnetic induction generator and triboelectric nanogenerator for harvesting mechanical energy. Adv Mater 2014;26:3580–91. https://doi.org/10.1002/adma.201400207.
[11] Wang ZL. Triboelectric nanogenerators as new energy technology and self-powered sensors - principles, problems and perspectives. Faraday Discuss 2014;176:447–58. https://doi.org/10.1039/C4FD00159A.
[12] Wang ZL, Wang A. On the origin of contact-electrification. Mater Today 2019;30:34–51. https://doi.org/10.1016/j.mattod.2019.05.016.
[13] Wang ZL. On Maxwell's displacement current for energy and sensors: the origin of nanogenerators. Mater Today 2017;20:74–82. https://doi.org/10.1016/j.mattod.2016.12.001.
[14] Xu C, Zi Y, Wang AC, Zou H, Dai Y, He Xu, et al. On the electron-transfer mechanism in the contact-electrification effect. Adv Mater 2018;30(15):1706790. https://doi.org/10.1002/adma.201706790.
[15] Wang ZL. Self-powered nanotech. Sci Am 2008;298:82–7. https://www.jstor.org/stable/26000379.
[16] Wang ZL, Jiang T, Xu L. Toward the blue energy dream by triboelectric nanogenerator networks. Nano Energy 2017;39:9–23. https://doi.org/10.1016/j.nanoen.2017.06.035.
[17] Cheng L, Xu Q, Zheng Y, Jia X, Qin Y. A self-improving triboelectric nanogenerator with improved charge density and increased charge accumulation speed. Nat Commun 2018;9:3773. https://doi.org/10.1038/s41467-018-06045-z.
[18] Xu L, Bu T, Yang X, Zhang C, Wang ZL. Ultrahigh charge density realized by charge pumping at ambient conditions for triboelectric nanogenerators. Nano Energy 2018;49:625–33. https://doi.org/10.1016/j.nanoen.2018.05.011.
[19] Mu J, Zou J, Song J, He J, Hou X, Yu J, et al. Xiujian Chou Hybrid enhancement effect of structural and material properties of the triboelectric generator on its performance in integrated energy harvester. Energy Convers Manag 2022;254:115151. https://doi.org/10.1016/j.enconman.2021.115151.
[20] Li Y, Zhao Z, Liu Lu, Zhou L, Liu Di, Li S, et al. Improved output performance of triboelectric nanogenerator by fast accumulation process of surface charges. Adv Energy Mater 2021;11(14):2100050. https://doi.org/10.1002/aenm.202100050.
[21] Liu W, Wang Z, Wang G, Liu G, Chen J, Pu X, et al. Integrated charge excitation triboelectric nanogenerator. Nat Commun 2019;10(1). https://doi.org/10.1038/s41467-019-09464-8.
[22] Wang H, Xu L, Bai Y, Wang ZL. Pumping up the charge density of a triboelectric nanogenerator by charge-shuttling. Nat Commun 2020;11:4203. https://doi.org/10.1038/s41467-020-17891-1.
[23] Wang H, Zhang M, Yang Z, Wang Z, Liu X, Lu Y, et al. Energy from greenhouse plastic films. Nano Energy 2021;89:106328. https://doi.org/10.1016/j.nanoen.2021.106328.
[24] Wang J, Yu X, Zhao Da, Yu Y, Gao Qi, Cheng T, et al. Enhancing output performance of triboelectric nanogenerator via charge clamping. Adv Energy Mater 2021;11(31):2101356. https://doi.org/10.1002/aenm.202101356.
[25] Satana P, Thitirat C, Nattapong P, Phieraya P, Wanwilai V, Phakkhananan P, et al. Triboelectric-piezoelectric hybrid nanogenerator based on BaTiO3-Nanorods/Chitosan enhanced output performance with self-charge-pumping system. Compos B Eng 2021;208:108602. https://doi.org/10.1016/j.compositesb.2020.108602.
[26] Ahmed H, Chengkuo L. Dielectric-elastomer-enhanced triboelectric nanogenerator with amplified outputs. Sens Actuator A Phys 2022;333:113270. https://doi.org/10.1016/j.sna.2021.113270.
[27] Chun J, Ye BU, Lee JW, Choi D, Kang C-Y, Kim S-W, et al. Boosted output performance of triboelectric nanogenerator via electric double layer effect. Nat Commun 2016;7(1). https://doi.org/10.1038/ncomms12985.
[28] Yang Z, Zhou S, Zu J, Inman D. High-performance piezoelectric energy harvesters and their applications. Joule 2018;2:642–97. https://doi.org/10.1016/j.joule.2018.03.011.
[29] Zou H, Zhang Y, Guo L, Wang P, He Xu, Dai G, et al. Quantifying the triboelectric series. Nat Commun 2019;10(1). https://doi.org/10.1038/s41467-019-09461-x.
[30] Wang Z, Liu W, He W, Guo H, Long Li, Xi Yi, et al. Ultrahigh electricity generation from low-frequency mechanical energy by efficient energy management. Joule 2021;5(2):441–55. https://doi.org/10.1016/j.joule.2020.12.023.
[31] Okbaz A, Karabiber A, Yar A, Kınas Z, Sarılmaz A, Ozel F. High-performance triboelectric nanogenerator with optimized Al or Ti-embedded silicone tribomaterial. Energy Convers Manag 2022;252:115053. https://doi.org/10.1016/j.enconman.2021.115053.
[32] Wu H, He W, Shan C, Wang Z, Fu S, Tang Q, et al. Achieving Remarkable Charge Density via Self-polarization of Polar High-k Material in Chargeexcitation Triboelectric Nanogenerator. Adv Mater 2109918. https://doi.org/10.1002/adma.202109918.
[33] Bai Yu, Xu L, Lin S, Luo J, Qin H, Han K, et al. Charge pumping strategy for rotation and sliding type triboelectric nanogenerators. Adv Energy Mater 2020;10(21):2000605. https://doi.org/10.1002/aenm.202000605.
[34] Liu Y, Liu W, Wang Z, He W, Tang Q, Xi Yi, et al. Quantifying contact status and the air-breakdown model of charge-excitation triboelectric nanogenerators to maximize charge density. Nat Commun 2020;11(1). https://doi.org/10.1038/s41467-020-15368-9.
[35] Long Li, Liu W, Wang Z, He W, Li G, Tang Q, et al. High performance floating self-excited sliding triboelectric nanogenerator for micro mechanical energy harvesting. Nat Commun 2021;12(1). https://doi.org/10.1038/s41467-021-25047-y.
[36] Yang Ze, Yang Y, Wang H, Liu F, Lu Y, Ji L, et al. Charge pumping for sliding-mode triboelectric nanogenerator with voltage stabilization and boosted Current. Adv Energy Mater 2021;11(28):2101147. https://doi.org/10.1002/aenm.202101147.
[37] Zhou L, Gao Y, Liu D, Liu L, Zhao Z, Li S, et al. Achieving ultrarobust and humidity-resistant triboelectric nanogenerator by dual-capacitor enhancement system. Adv Energy Mater 2021; 2101958. https://doi.org/10.1002/aenm.202101958.
[38] Wang K, Weng Y, Chen G, Wu C, Park J, Qiu Z, et al. Coupling electrostatic induction and global electron circulation for constant-current triboelectric nanogenerators. Nano Energy 2021;85:105929. https://doi.org/10.1016/j.nanoen.2021.105929.
[39] Ding R, Cao Z, Wu Z, Xing H, Ye X. All-in-One High output rotary electrostatic nanogenerators based on charge pumping and voltage multiplying. ACS Nano 2021;15:16861–9. https://doi.org/10.1021/acsnano.1c07480.
[40] Satana P, Phakkhananan P, Thitirat C, Naratip V. Low-cost fabrication of the highly efficient triboelectric nanogenerator by designing a 3D multi-layer origami structure combined with self-charged pumping module. Nano Energy 2021;90:106629. https://doi.org/10.1016/j.nanoen.2021.106629.
[41] Fu S, He W, Tang Q, Wang Z, Liu W, Li Q, et al. An Ultrarobust and High-Performance Rotational Hydrodynamic Triboelectric Nanogenerator Enabled by Automatic Mode Switching and Charge Excitation. Adv Mater 2022;34(2):2105882. https://doi.org/10.1002/adma.202105882.
[42] Niu S, Zhou Y, Wang S, Liu Y, Lin L, Bando Y, et al. Simulation method for optimizing the performance of an integrated triboelectric nanogenerator energy harvesting system. Nano Energy 2014;8:150–6. https://doi.org/10.1016/j.nanoen.2014.05.018.
[43] Xu S, Zhang L, Ding W, Guo H, Wang X, Wang ZL. Self-doubled-rectification of triboelectric nanogenerator. Nano Energy 2019;66:104165. https://doi.org/10.1016/j.nanoen.2019.104165.
[44] Zhao D, Yu X, Wang Z, Wang J, Li X, Wang ZL, et al. Universal equivalent circuit model and verification of current source for triboelectric nanogenerator. Nano Energy 2021;89:106335. https://doi.org/10.1016/j.nanoen.2021.106335.

Dr. Xin Yu is a lecturer in the College of Electrical and Electronic Engineering, Changchun University of Technology. He obtained the B.S. and Ph.D. degrees from Jilin University in 2009 and 2014, respectively. He was a visiting scholar at Michigan State University from 2017 to 2018, and he is a visiting scholar in Beijing Institute of Nanoenergy and Nanosystems, Chinese Academy of Sciences, currently. His interests are triboelectric nanogenerators, infrared gas sensing, and photoelectric information detection.

Jianwei Ge received the B.E. degree from the School of Electrical and Electronic Engineering Changchun University of Technology in 2020. He is currently working toward the M.S. degree in energy and power at the same school. He is currently a visiting student in Beijing Institute of Nanoenergy and Nanosystems. His interests are triboelectric nanogenerators, self-powered sensor, and energy harvester.

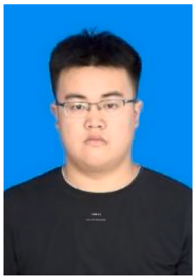

Zhenjie Wang was born in Hubei Province, China, in 1998. He received a B.E. degree from North China Institute of Science and Technology in Hebei Province, China, in 2019. He is currently studying for a master's degree in the School of Electrical and Electronic Engineering, Changchun University of Technology, and is a visiting student in Beijing Institute of Nanoenergy and Nanosystems. His interests are triboelectric nanogenerators, infrared gas sensing, and photoelectric detection.

Jianlong Wang was born in 1996 Shandong Province, majored in mechanical engineering and received his B.E. degree from Changchun University of Technology. He is currently a master degree candidate under the supervision of Prof. Tinghai Cheng in the same school. His research interest is in the area of triboelectric nanogenerators.

Da Zhao received the M.S. degree from Changchun University of Technology, China, in 2020. He is currently studying for his Ph.D. degree in School of Mechatronic Engineering at Changchun University of Technology, and is also a visiting student in Beijing Institute of Nanoenergy and Nanosystems. His research interests focus on triboelectric nanogenerators and piezoelectric energy harvester.

Prof. Zhong Lin Wang received his Ph.D. from Arizona State University in physics. He now is the Hightower Chair in Materials Science and Engineering, Regents' Professor, Engineering Distinguished Professor and Director, Center for Nanostructure Characterization, at Georgia Tech. Dr. Wang has made original and innovative contributions to the synthesis, discovery, characterization and understanding of fundamental physical properties of oxide nanobelts and nanowires, as well as applications of nanowires in energy sciences, electronics, optoelectronics and biological science. His discovery and breakthroughs in developing nanogenerators established the principle and technological road map for harvesting mechanical energy from environment and biological systems for powering personal electronics. His research on self-powered nanosystems has inspired the worldwide effort in academia and industry for studying energy for micro-nano-systems, which is now a distinct disciplinary in energy research and future sensor networks. He coined and pioneered the field of piezotronics and piezophototronics by introducing piezoelectric potential gated charge transport process in fabricating new electronic and optoelectronic devices. Details can be found at: http:// www.nanoscience.gatech.edu.

Prof. Tinghai Cheng received the B.S., M.S. and Ph.D. degrees from Harbin Institute of Technology in 2006, 2008 and 2013, respectively. He was a visiting scholar in School of Materials Science and Engineering at Georgia Institute of Technology from 2017 to 2018. Currently, he is a professor of Beijing Institute of Nanoenergy and Nanosystems, Chinese Academy of Sciences. His research interests are piezoelectric actuators, piezoelectric energy harvester, and triboelectric nanogenerators.